

RSC Advances



This is an *Accepted Manuscript*, which has been through the Royal Society of Chemistry peer review process and has been accepted for publication.

Accepted Manuscripts are published online shortly after acceptance, before technical editing, formatting and proof reading. Using this free service, authors can make their results available to the community, in citable form, before we publish the edited article. This *Accepted Manuscript* will be replaced by the edited, formatted and paginated article as soon as this is available.

You can find more information about *Accepted Manuscripts* in the [Information for Authors](#).

Please note that technical editing may introduce minor changes to the text and/or graphics, which may alter content. The journal's standard [Terms & Conditions](#) and the [Ethical guidelines](#) still apply. In no event shall the Royal Society of Chemistry be held responsible for any errors or omissions in this *Accepted Manuscript* or any consequences arising from the use of any information it contains.

ARTICLE

Facile preparation of C-modified TiO₂ supported on MCF for high visible-light-driven photocatalysis

Cite this: DOI: 10.1039/x0xx00000x

Bocheng Qiu^a, Chengchao Zhong^a, Mingyang Xing^{*a} and Jinlong Zhang^{*a, b}Received 00th January 2012,
Accepted 00th January 2012

DOI: 10.1039/x0xx00000x

www.rsc.org/

A green and facile approach is employed to prepare an efficient visible-light-driven photocatalyst by using mesocellular foams (MCF) as matrix, glucose as a carbon-modified source and TiO₂ as the catalytic active sites, which is denoted as C-modified TiO₂/MCF. Characterization results reveal that nano-sized TiO₂ nanoparticles are loaded in the pore channels of MCF rather than aggregated on the surface of MCF. Furthermore, glucose is selectively covered on the surface of TiO₂/MCF composites during the stirring process due to the excellent adsorption capacity of MCF, and then glucose can be transformed to the coke carbon through a hydrothermal process. In addition, a facile thermal treatment is adopted to enhance the visible light photocatalytic activity of TiO₂/MCF composites. It is believed that the post-thermal treatment plays a significant role in controlling the carbon diffusion from the surface to the bulk of TiO₂. Compared to traditional C-TiO₂ photocatalyst, the prepared C-doped catalyst exhibits a stable carbon doping in TiO₂, more excellent adsorption capacity and higher visible light photocatalytic activity owing to the special structure of supported mesoporous catalyst. This study implies that the novel photocatalyst has a large application prospect in photocatalytic water splitting, dye-sensitized solar cell and other fields.

1. Introduction

Titanium dioxide (TiO₂) has been widely studied as a well-known photocatalyst due to its advantages of non-toxicity, excellent stability, low materials cost.¹⁻⁸ As TiO₂ only absorbs ultraviolet light energy which only accounts for ca.4% of the solar spectrum,⁹⁻¹¹ many efforts have been focused on improving the visible light photocatalytic performance of TiO₂, such as element doping,^{12, 13} oxygen deficiency¹⁴⁻¹⁶ and compositing.¹⁷⁻¹⁹ Especially, carbon doping can significantly enhance visible-light absorption and energy conversion, and stabilize anatase TiO₂.^{20, 21} Except for that, carbon doping can also improve the conductivity of TiO₂, as it could facilitate the charge from the bulk of TiO₂ to the surface region.²² Khan et al.²³ reported the high photoactivity of C-doped TiO₂ in the photoelectrochemical water splitting reaction to produce H₂ and O₂, and obtained photo-conversion efficiency as high as 8.35%. Similarly, Kisch et al.²⁴ verified that C-doped TiO₂ could efficiently mineralize 4-chlorophenol and the azo dye remazol red under indoor light, whereas unmodified TiO₂ was almost inactive.

However, there still exists some instant shortages to decrease the visible light activity. The major problems are focused on: 1) most of the carbon is loaded on the surface of TiO₂ rather than in the bulk and the carbon existed on the surface is easy to fall off in the photocatalytic reaction, leading to the catalyst

deactivation; 2) the doping of carbon into the lattice of TiO₂ usually results in the formation of oxygen vacancies in the bulk and these defects can induce charge trapping and recombination sites of photo-excited charge carriers.^{22, 25-27} Recently, mesoporous materials are widely used as matrix to support the metal or nonmetal oxides and an ideal adsorbent to adsorb the organic pollutants,²⁸⁻³¹ owing to their controllable pore size and large specific surface area. Mesoporous materials could offer separated space for crystalline TiO₂ and adsorb more carbon species on the surface of TiO₂ in the hydrothermal process. That is, the coke carbon covered on the surface of TiO₂ is difficult to drop into the reaction system during the photocatalytic reaction process due to the protection of the mesoporous structure.

Herein, we employed a green and novel approach for the fabrication of catalyst integrated with C-modified TiO₂ by using MCF as the matrix through the hydrothermal and post-thermal processes. The MCF matrices can provide abundant sites and spaces for the loading of TiO₂ nanoparticles and the location of glucose. In this case, the TiO₂ nanoparticles nucleated, grew, and crystallized in the pore channels of MCF, and C₆H₁₂O₆ was adsorbed, transformed and doped into lattice of TiO₂, which are precisely separated and controlled via the hydrothermal and post-thermal processes. The prepared C-modified TiO₂/MCF composites not only possessed highly dispersed TiO₂ nanoparticles (~10 nm) and a high surface area

of $\sim 389.79 \text{ m}^2 \text{ g}^{-1}$, but also exhibited excellent visible light photocatalytic activity in degradation of methyl orange.

2. Experimental-materials and methods

2.1 Materials

All chemicals, including pluronic P123 triblock copolymer (EO20PO70EO20, $M_{av} = 5800$, Aldrich), 1, 3, 5-trimethylbenzene (TMB, AR), ammonium fluoride (AR), tetraethyl orthosilicate (TEOS, AR), hydrochloric acid (HCl, 36-38%), titanium sulfate (CP), glucose (AR) were used as received without any further purification.

2.2 Preparation of MCF

The pure siliceous MCF sample was prepared as described previously.³² In detail, 4.0 g P123 was dissolved in the mixture solution of 20 mL HCl and 130 mL distilled water under the 37 °C temperature. 46.7 mg NH_4F and 2.0 g TMB were added in the above solution under vigorous stirring for 1 hour. Then, the temperature of the system rose to 37 °C and 18.3 mL TEOS was slowly added dropwise into the above solution. The mixture solution was kept at 37 °C with stirring for 20 hours. The obtained slurry was transferred to an autoclave and aged at 100 °C for another 24 hours. The solid products were washed by the distilled water and dried overnight at 60 °C under vacuum conditions. The occluded surfactant was removed by calcination in a muffle furnace at 550 °C for 6 h in air. The final products were obtained and denoted as MCF.

2.3 Preparation of C-modified TiO_2/MCF

3 g $\text{Ti}(\text{SO}_4)_2$ and a certain amount of glucose were dissolved into 63 mL distilled water under the stirring for 30 minutes. 2 g MCF was added into the solution and string for 30 minutes. The solution was transferred to an autoclave and kept at 120 °C for 7 hours. The obtained products were washed and dried at 60 °C for 12 hours under the vacuum conditions to obtain the catalyst of MCF loaded with C-modified TiO_2 . The obtained composites were denoted as “nC- TiO_2/MCF ” (“n” indicates the amount of glucose, n=0.1, 0.20, 0.40, 0.80, 1.20, 1.60 g). To investigate the effect of post-thermal treatment on C- TiO_2/MCF , the as-prepared C- TiO_2/MCF was treated in air at 200 °C, 300 °C, and 400 °C for 2 h in a muffle furnace, respectively. The corresponding samples were labeled as nC- TiO_2/MCF -200, nC- TiO_2/MCF -300, and nC- TiO_2/MCF -400, respectively. The as prepared sample without addition of glucose was denoted as TiO_2/MCF .

2.4 Characterization

X-ray diffraction (XRD) patterns of all samples were collected in the range 10-80° (2 θ) using a RigakuD/MAX 2550 diffractometer (Cu K radiation, $\lambda = 1.5406 \text{ \AA}$), operated at 40 kV and 100 mA. The morphologies were characterized by transmission electron microscopy (TEM, JEM2000EX). The ground samples for TEM measurements were suspended in ethanol with the assist of ultrasound and supported on a carbon-coated copper grid. The instrument employed for XPS studies was a Perkin-Elmer PHI 5000C ESCA system with Al K α radiation operated at 250 W. The shift of the binding energy due to relative surface charging was corrected using the C1s level at 284.4 eV as an internal standard. The UV-Vis absorption spectra of samples were observed with (Varian Cary 500) equipped with an integrating sphere. N_2

adsorption/desorption isotherms were measured on an ASAP2020 instrument at 77 K. Before the measurements, all samples were degassed at 180 °C for 8 h. Raman spectra were collected by using Raman microscopes (Renishaw, UK) under a 514 nm excitation.

2.5 Photoelectrochemical Tests

Photocurrent measurements were carried out with an analyzer (Zahner, Zennium) in dark conditions using a standard three electrode cell with a working electrode, a Pt wire as the counter electrode, and a saturated calomel electrode as the reference electrode. A 0.5 M solution of Na_2SO_4 was used as the electrolyte.

2.6 Photocatalytic Activity Tests

The photocatalytic reaction details are as followings. All experiments are conducted at normal temperatures and pressures. The photocatalytic activity of the prepared samples is evaluated by the photocatalytic degradation of methyl orange (MO) under visible light irradiation. Briefly, 70 mg of catalyst and 70 mL of MO solution (10 mg/L) were added together into the reaction tube equipped with a magnetic stirrer, exposed to a 500 W tungsten halogen lamp equipped with a UV cut-off filters ($\lambda > 420 \text{ nm}$). The distance between the light and the reaction tube was fixed at 24 cm. Before the irradiation, the suspension was maintained in the dark for 2 h in order to reach the adsorption-desorption equilibrium. When the first photocatalytic reaction was finished, the solid catalyst was recovered by centrifugation, re-dispersed in water and irradiated for 30 min to degrade the residual MO adsorbed on the surface of TiO_2 . Then, the catalyst was recovered by centrifugation, washed three times with deionized water, dried under vacuum at 40 °C, and subjected to the next photocatalytic reaction in recycle tests. Every cycle, we will use a new MO solution (10 mg/L), thus we can eliminate the impact of residual MO on the cycle tests.

3. Results and discussion

The C-modified TiO_2/MCF was prepared via the hydrothermal and post-thermal method (Fig. 1). During the hydrothermal process, the carbon source ($\text{C}_6\text{H}_{12}\text{O}_6$) could be quickly adsorbed into the pore channels of MCF and covered on the surface of TiO_2 , and then was turned into the coke carbon. The next post-thermal processes could facilitate part of coke carbon moving from surface to bulk of TiO_2 (Fig. 1). The obtained composites were denoted as “nC- TiO_2/MCF -T” (“n” indicates the addition amount of glucose, n=0.1, 0.20, 0.40, 0.80, 1.20, 1.60 g; “T” indicates the thermal treatment temperature, T=100, 200, 300 °C). The composites without thermal treatment were denoted as “nC- TiO_2/MCF ”. The pure $\text{Ti}(\text{SO}_4)_2$ and MCF without the addition of $\text{C}_6\text{H}_{12}\text{O}_6$ through hydrothermal process were denoted as TiO_2/MCF .

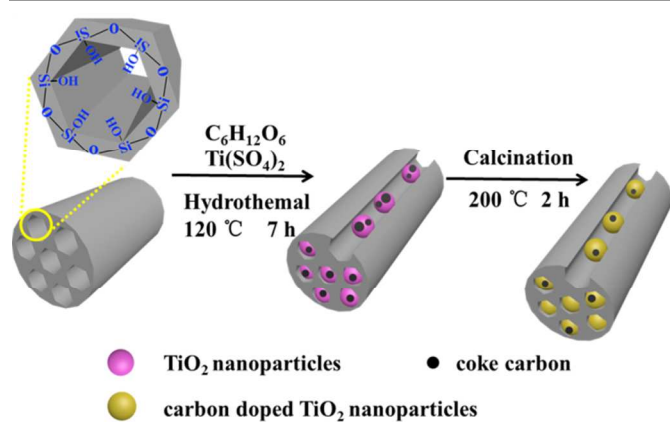


Fig. 1 Fabrication process for C-TiO₂/MCF composites

3.1 Nanoparticle crystal structure and specific surface area

The morphology and structure of C-TiO₂/MCF composites are first examined by X-ray diffraction (XRD) (Fig. 2a). All the samples are pure anatase phase with the uniform crystals of 10 nm in size calculated by the Scherrer equation. That means the pore size of MCF must be much larger than 10 nm to ensure the TiO₂ nanoparticles loading into the pore channels of MCF. Indeed, this is supported by the pore channels diameter of the MCF (20-50 nm) (Fig. 2b, inset). In addition, with the increasing addition of C₆H₁₂O₆ and the variation of thermal treatment temperature, the size of crystal is almost unchanged. That is, the addition of C₆H₁₂O₆ and the process of the thermal treatment cannot affect the size of crystal. The nitrogen physisorption measurements indicate the pore size of MCF is around in the range of 20-50 nm (Fig. 2b), which implies the entire possibility of TiO₂ nanoparticles introducing into the pore channels of MCF. The adsorption data reveal a remarkably high specific surface area of 548.97 m² g⁻¹ for MCF. With the occupation of the TiO₂ nanoparticles inside the mesoporous channels, a significant decrease of the surface area from 548.97 to 416.19 m² g⁻¹ and a decrease of the range of pore size from 20-50 nm to 10-40 nm are observed for the TiO₂/MCF catalyst (Fig. 2c), which can be ascribed to the fact that TiO₂ nanoparticles are introduced into the pore channels rather than covered on the surface of MCF. Compared with TiO₂/MCF, although the surface area of 1.2C-MCF/TiO₂ has a slight decrease to 389.79 m² g⁻¹ (Fig. 2d), the range of pore size and the shape of the N₂ sorption isotherms are almost unchanged, which implies the successful introduction of C₆H₁₂O₆ into the pore channels of MCF rather than outside of MCF.

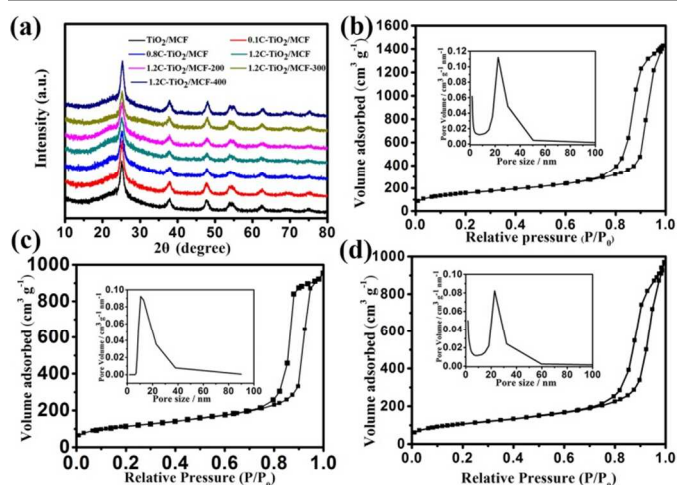


Fig. 2 XRD patterns for C-TiO₂/MCF composites (a) and N₂ sorption isotherms of (b) MCF, (c) TiO₂/MCF, (d) 1.2C-TiO₂/MCF (inset: pore size distribution).

3.2 Investigation of the carbon existential form

To investigate the carbon existential form in the series of C-TiO₂/MCF composites, we conducted the X-ray photoelectron spectroscopy (XPS), Raman spectroscopy and UV-vis absorption spectra on samples. The C-1s XPS spectra of 1.2C-TiO₂/MCF, 1.2C-TiO₂/MCF-200 and 1.2C-TiO₂/MCF-400 are shown in Fig. 3a. A broad energy range from 280.0 to 294.0 eV can be observed. The peak at 284.6 eV among the three samples is assigned to the adventitious carbon species from the XPS measurement. The peak at 289.0 eV for both 1.2C-TiO₂/MCF and 1.2C-TiO₂/MCF-200 belongs to the C(O)OH bond. It means that larger amounts of C(O)OH species exist on the catalyst surface. From the Raman spectra (Fig. 3b), the two peaks at 1400 cm⁻¹ and 1600 cm⁻¹ of 1.2C-TiO₂/MCF and 1.2C-TiO₂/MCF-200 are from the coke carbon species.^{33, 34} Therefore, the surface C(O)OH species deduced from XPS spectra analysis are coke carbon species covered on the surface. Some research works also showed that surface-bonded coke carbon was very easy to generate when glucose was used as the carbon source.³⁵ Comparing the two peaks intensity of 1.2C-TiO₂/MCF and 1.2C-TiO₂/MCF-200 respectively (Fig. 3b), we can find that part of the coke carbon species are doped into the bulk of TiO₂, which leads to a reduction of intensity and a slight color change for 1.2C-TiO₂/MCF-200 (Fig. 3d). Furthermore, the peak at 282.0 eV for 1.2C-TiO₂/MCF-200 is caused by O-Ti-C bond³⁶, which is a convenient indicator of successful carbon doping into the lattice of TiO₂. Interestingly, these peaks for the surface coke carbon and the bulk carbon in XPS and Raman spectra are disappearing when the thermal treatment temperature is up to 400 °C. Obviously, the higher temperature will result in an entire loss of both the surface coke carbon and the bulk carbon. Fig. 3c clearly shows the UV-Vis absorption spectra for the undoped TiO₂/MCF, 1.2C-TiO₂/MCF and the thermal treated composites. The undoped TiO₂/MCF only has absorption in UV region, but the thermally treated composites of 1.2C-

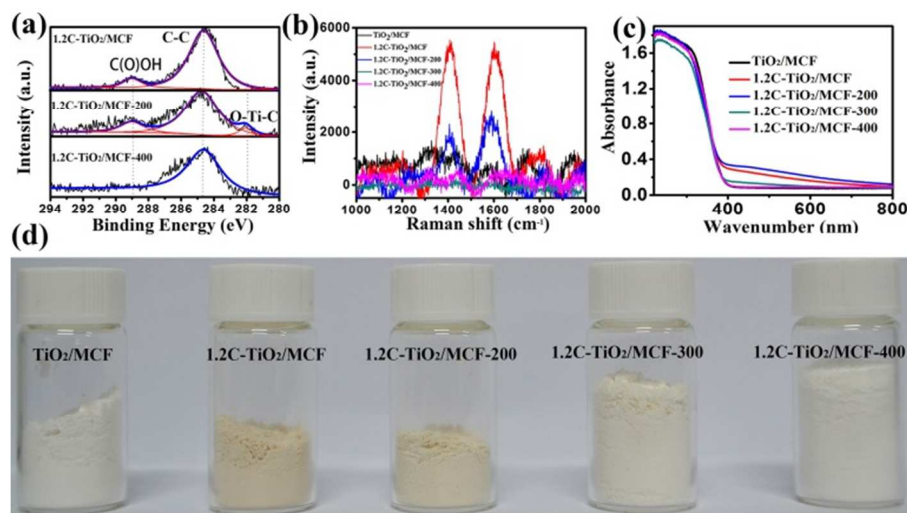


Fig. 3 XPS spectra of pristine and thermal-treated C-TiO₂/MCF (a); Raman spectra of pristine and thermal-treated C-TiO₂/MCF (b); C-TiO₂/MCF UV-Vis absorption spectra for different samples (c); Photographs of as prepared samples (d).

TiO₂/MCF-200 extends absorption from the UV region to the visible light region. Nevertheless, the thermally treated samples at 400 °C only absorb UV light, which is the same as the undoped TiO₂/MCF. These results indicate the existence of the carbon from the surface to the bulk for the 1.2C-TiO₂/MCF-200 samples. Both the 1.2C-TiO₂/MCF and 1.2C-TiO₂/MCF-200 samples display apparent color change to light yellow from white TiO₂/MCF (Fig. 3d), which is caused by the surface coke carbon. This result suggests that the treatment temperature being close to 200 °C will not lead to a big loss of surface carbon. The sample treated at 400 °C is pure white. These results are in good agreement with the results of XPS.

3.3 Nanoparticle morphology

The transmission electron microscopy (TEM) images of MCF, TiO₂/MCF, 1.2C-TiO₂/MCF, 1.2C-TiO₂/MCF-200 are shown in Fig. 4. The mesopore channels of MCF could be observed with the size ranging from 20 to 50 nm (Fig. 4a), agreeing well with the BET result. After the hydrothermal process, the TiO₂ nanoparticles were introduced into the pore channels of MCF, which is well consistent with the observation that there is absence of aggregated TiO₂ nanoparticles covered on the surface of MCF (Fig. 4b). Our previous work on TiO₂/MCF also has demonstrated that the TiO₂ nanoparticles are indeed loaded into the pore channels rather than covered on the surface of MCF.⁶ Meanwhile, the mesoporous structure is clearly observed after hydrothermal reaction with the addition of C₆H₁₂O₆ (Fig. 4c). These results suggest that the C₆H₁₂O₆ can

be selectively adsorbed into the mesopore channels without free covered outside of the pore channels. Through the thermal treatment of 1.2C-TiO₂/MCF sample in the air at 200 °C, the mesoporous structures are not destroyed and the pore size is almost changeless (Fig. 4d). In addition, the high-resolution transmission electron microscope (HRTEM) image (Fig. 4e) of 1.2C-TiO₂/MCF clearly shows the mesoporous structure with an average pore diameter centered at 20–40 nm, which is in good agreement with the BET results. In addition, the HRTEM image (Fig. 4f) demonstrates that highly crystalline TiO₂ nanoparticles are selectively loaded in the pore channels of MCF. A well-defined crystalline lattice can be identified with a d spacing of 0.35 nm corresponding to the (101) plane of anatase TiO₂.

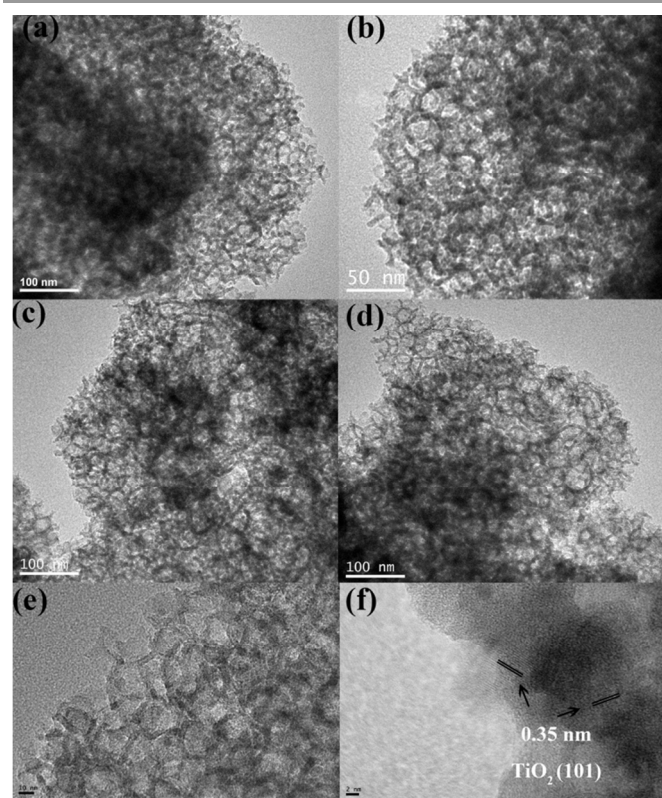


Fig. 4 TEM images for different samples. (a) MCF, (b) TiO₂/MCF, (c) 1.2C-TiO₂/MCF, (d) 1.2C-TiO₂/MCF-200. HRTEM images (e, f) for 1.2C-TiO₂/MCF-200.

3.4 Effect of the addition amount of C₆H₁₂O₆ and thermal treatment on the photocatalytic activity

The photocatalytic activity of the as-prepared samples is evaluated by the degradation of methyl orange (MO 10 mg/L) under visible light irradiation ($\lambda > 420$ nm). Firstly, we investigated the effect of C₆H₁₂O₆ addition amount on the photocatalytic activity of C-TiO₂/MCF composites. Fig. 5a shows adsorption capacity of MO in the dark for C-TiO₂/MCF treated at different addition amount of C₆H₁₂O₆. It can be seen that all the C-TiO₂/MCF composites exhibit an excellent adsorption capacity of MO in the dark for 2 h due to the existence of mesoporous structure (MCF). However, with the increasing addition of C₆H₁₂O₆, the photodegradation rate of MO over C-TiO₂/MCF composites under the visible light irradiation increases first and then decreases obviously (Fig. 5b). When the C₆H₁₂O₆ addition amount was 1.2 g, the corresponding catalyst demonstrated the optimal photocatalytic activity. Analogous activity trend for photocatalytic reaction is also observed over the C-TiO₂ nanocomposites in some other previous reports.³⁷ The value of the degradation rate of MO for 1.2C-TiO₂/MCF is around 60% after under the visible light irradiation for 5 h, which is related to the amount of the surface coke carbon on TiO₂. It further confirms that the high photocatalytic activity for 1.2C-TiO₂/MCF is ascribed to photosensitization mechanism of surface coke carbon. When

the amount of the surface coke carbon is beyond the optimum addition, excess surface carbon will wrap the TiO₂ surface and the electron generated from photosensitization is very difficult to reach the conductive band (CB) of TiO₂, which leads to a relatively lower photoactivity of 1.6C-TiO₂/MCF than that of 1.2C-TiO₂/MCF. In order to eliminate the effect of the dye self-sensitization, the photocatalytic reaction in the absence of catalyst has been investigated (Figure 5b). It can be seen that the effect of the dye self-sensitization is very weak, which further confirms that the high photocatalytic activity for 1.2C-TiO₂/MCF is attributed to the photosensitization mechanism of surface coke carbon. To the catalyst of 1.2C-TiO₂/MCF treated at 100-300 °C, the adsorption capacity of MO in the dark is no difference among the three samples (Fig. 5c). Under the optimized thermal treatment condition, 1.2C-TiO₂/MCF-200 exhibited the highest photocatalytic activity. After visible light illumination for 5 h, the MO can be degraded up to 80% by 1.2C-TiO₂/MCF-200, higher than the 1.2C-TiO₂/MCF catalyst (Fig. 5d). However, both 1.2C-TiO₂/MCF-300 and 1.2C-TiO₂/MCF-400 show lower photocatalytic activity than the pristine 1.2C-TiO₂/MCF, which is ascribed to the absence of carbon in the bulk or on the surface at a high temperature calcination treatment. This result is consistent with the previous report.²⁰

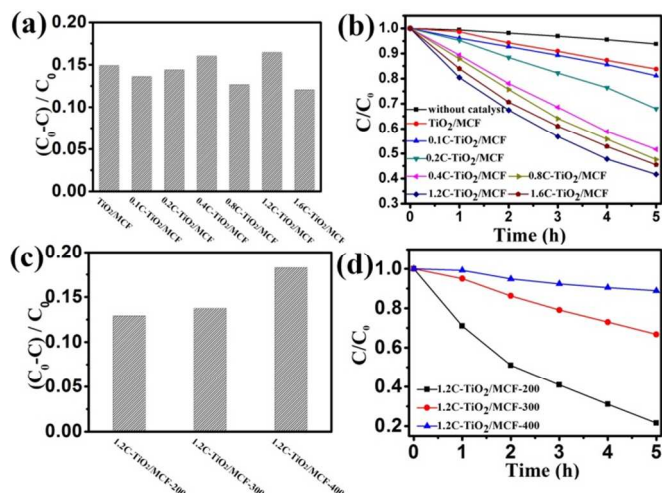


Fig. 5 Adsorption capacities of MO (10 mg/L) for different samples (a, c); Visible light photocatalytic activities of different samples (b, d).

3.5 The stability of the catalyst in the cycle photocatalytic performance

To examine the photocatalytic stability of C-TiO₂/MCF-200, We performed visible-light-driven degradation of MO (10 mg/L) cycle experiments. As shown in Fig. 6a, the catalyst maintains high photodegradation rate of MO (80%), without an apparent decrease after five cycles. Additionally, the XPS spectra of C-TiO₂/MCF-200 after five cycles show that the Ti-O-C bond and the surface C(O)OH species still exist in the

catalyst (Fig. 6b). More direct observations by HRTEM on morphology and structure of C-TiO₂/MCF-200 after five cycles is shown in Fig. 6c. The mesoporous structure can still be retained and the pore diameter keeps the initial size. This result also indicates that the prepared C-TiO₂/MCF-200 has a very stable structure.

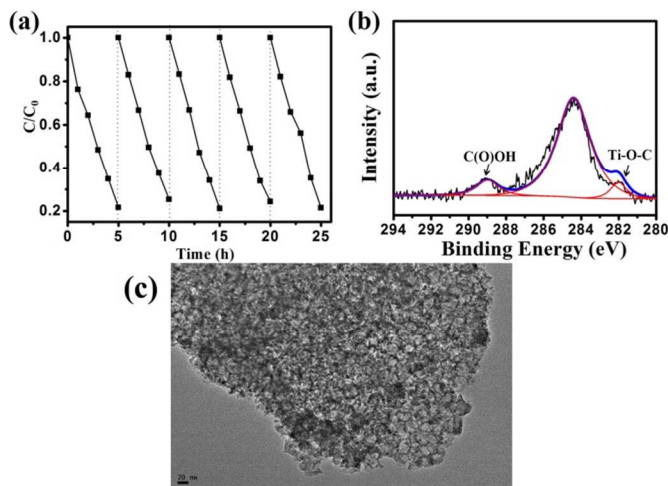


Fig. 6 Cycling photodegradation of MO for C-TiO₂/MCF-200 (a); The XPS spectra of C-TiO₂/MCF-200 after 5 cycles (b); The HRTEM image of C-TiO₂/MCF-200 after 5 cycles (c).

3.6 Effect of thermal treatment on photoelectrochemical properties

In order to further investigate the photoelectrochemical properties, we have used the transient photocurrent response measurements to characterize the lifetime and transfer rate of photogenerated electron-hole pairs. The photocurrents of these samples were recorded in dark or in the visible light illumination from a xenon lamp assembled a 420 nm optical filter, as shown in Fig. 7a. The transient photocurrent response measurements show that the photocurrent of 1.2C-TiO₂/MCF-200 is much higher than that of other samples, verifying the lowest recombination efficiency of photogenerated electron-hole pairs. The improvement of photocurrent density is caused by the thermal treatment, which can promote the carbon from surface to bulk and decrease the surface defects. In the contrast, under visible light illumination, the 1.2C-TiO₂/MCF-300 and 1.2C-TiO₂/MCF-400 electrodes all give a significant decrease of photocurrent density, compared to 1.2C-TiO₂/MCF. That is, once the thermal treatment temperature is more than the optimum value, it will cause the catalyst to lose the surface carbon and the doping carbon species. When the temperature reaches up to 400 °C, all the carbon no matter covered on surface or doped in the bulk of TiO₂ will be burn off. The result of transient photocurrent responses is well in accordance with the photocatalytic activity result. Hence, we can conclude that the synergistic effect between carbon doping and surface carbon coverage is the key to increase the solar absorption and

photocatalytic activity of 1.2C-TiO₂/MCF-200 composites. The presence of Ti-C bond indicates the oxygen atoms in TiO₂ are substituted by C atoms and a narrow substitute band is formed above valence band (VB) (Fig. 7b). The photogenerated electrons easily transfer from the carbon dopant level to the conducted band (CB). Simultaneously, under the visible light illumination, the photogenerated electrons transfer from coke carbon to the CB of TiO₂ as shown in Fig. 7b. The electrons and holes further react with O₂ or H₂O to generate the active groups such as the superoxide radical and hydroxyl radicals, which is responsible for the observed high photocatalytic activity of 1.2 C-TiO₂/MCF-200.

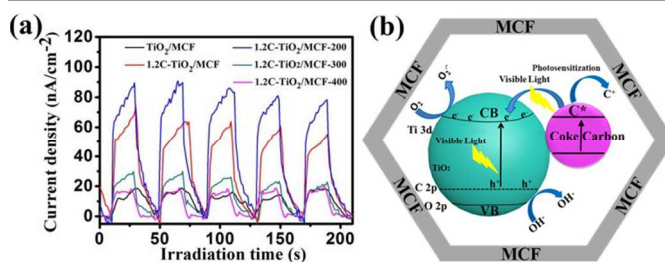


Fig. 7 Transient photocurrent responses for different samples (a); Schematic representation of the photocatalytic reaction on C-TiO₂/MCF-200 (b).

4. Conclusions

In summary, we have employed the hydrothermal and thermal treatment method to prepare an efficient visible-light-driven C-modified TiO₂/MCF photocatalyst. This method can bring about dramatic changes in their structural, optical, electronic and chemical properties. This C-modified TiO₂/MCF composites have displayed much higher photocatalytic activities than the TiO₂/MCF composites due to the synergistic effect between the reduction of band gap caused by the doped carbon and the photosensitization caused by the surface carbon. We believe that the novel photocatalyst has a large application prospect in photocatalytic water splitting, dye-sensitized solar cell, air purification and other fields.

Acknowledgements

This work has been supported by the National Natural Science Foundation of China (21203062, 21173077, 21377038, 21237003), the National Basic Research Program of China (973 Program, 2013CB632403), the Research Fund for the Doctoral Program of Higher Education (20120074130001) and the Fundamental Research Funds for the Central Universities.

Notes and references

^aKey Laboratory for Advanced Materials and Institute of Fine Chemicals, East China University of Science and Technology, 130 Meilong Road, Shanghai 200237, P.R. China

^bDepartment of Chemistry, Tsinghua University, Beijing 100084, P. R. China
*Corresponding Author: Email: mingyangxing@ecust.edu.cn; jlzhang@ecust.edu.cn

1. Y. Park, W. Kim, H. Park, T. Tachikawa, T. Majima and W. Choi, *Appl. Catal. B: Environ.*, 2009, **91**, 355-361.
2. M. Xing, J. Zhang, F. Chen and B. Tian, *Chem. Commun.*, 2011, **47**, 4947-4949.
3. T. Kamegawa, S. Matsuura, H. Seto and H. Yamashita, *Angew. Chem. Int. Ed.*, 2013, **52**, 916-919.
4. N. Sakaguchi, S. Matsuo, T. Kurisaki, T. Matsuo and H. Wakita, *Res. Chem. Intermed.*, 2006, **32**, 95-101.
5. C. Yang, Z. Wang, T. Lin, H. Yin, X. Lü, D. Wan, T. Xu, C. Zheng, J. Lin, F. Huang, X. Xie and M. Jiang, *J. Am. Chem. Soc.*, 2013, **135**, 17831-17838.
6. M. Xing, J. Zhang, B. Qiu, B. Tian, M. Anpo and M. Che, *Small*, 2014, DOI: 10.1002/sml.201403056.
7. J. Yu, J. Low, W. Xiao, P. Zhou and M. Jaroniec, *J. Am. Chem. Soc.*, 2014, **136**, 8839-8842.
8. J. Schneider, M. Matsuoka, M. Takeuchi, J. Zhang, Y. Horiuchi, M. Anpo and D. W. Bahnemann, *Chem. Rev.*, 2014, **114**, 9919-9986.
9. X. Chen, S. Shen, L. Guo and S. S. Mao, *Chem. Rev.*, 2010, **110**, 6503-6570.
10. R. Bauer and H. Fallmann, *Res. Chem. Intermed.*, 1997, **23**, 341-354.
11. H. Zhang, X. Lv, Y. Li, Y. Wang and J. Li, *ACS nano*, 2009, **4**, 380-386.
12. R. Asahi, T. Morikawa, T. Ohwaki, K. Aoki and Y. Taga, *Science*, 2001, **293**, 269-271.
13. M. Takeuchi, M. Matsuoka and M. Anpo, *Res. Chem. Intermed.*, 2012, **38**, 1261-1277.
14. Z. Lin, A. Orlov, R. M. Lambert and M. C. Payne, *J. Phys. Chem. B*, 2005, **109**, 20948-20952.
15. G. Liu, H. G. Yang, X. Wang, L. Cheng, H. Lu, L. Wang, G. Q. Lu and H.-M. Cheng, *J. Phys. Chem. C*, 2009, **113**, 21784-21788.
16. I. Nakamura, S. Sugihara and K. Takeuchi, *Chem. Lett.*, 2000, **29**, 1276-1277.
17. B. Qiu, M. Xing and J. Zhang, *J. Am. Chem. Soc.*, 2014, **136**, 5852-5855.
18. M. Xing, X. Li and J. Zhang, *Sci. Rep.*, 2014, **4**, 5493-5499.
19. T. H. Kim, C. Gómez-Solis, E. Moctezuma and S. W. Lee, *Res. Chem. Intermed.*, 2014, **40**, 1595-1605.
20. I.-C. Kang, Q. Zhang, S. Yin, T. Sato and F. Saito, *Appl. Catal. B: Environ.*, 2008, **80**, 81-87.
21. D. Qi, M. Xing and J. Zhang, *J. Phys. Chem. C*, 2014, **118**, 7329 - 7336
22. F. Dong, S. Guo, H. Wang, X. Li and Z. Wu, *J. Phys. Chem. C*, 2011, **115**, 13285-13292.
23. S. U. M. Khan, M. Al-Shahry and W. B. Ingler, *Science*, 2002, **297**, 2243-2245.
24. S. Sakthivel and H. Kisch, *Angew. Chem. Int. Ed.*, 2003, **42**, 4908-4911.
25. Y. Cong, J. Zhang, F. Chen, M. Anpo and D. He, *J. Phys. Chem. C*, 2007, **111**, 10618-10623.
26. J. Zhang, Y. Wu, M. Xing, S. A. K. Leghari and S. Sajjad, *Energy Environ. Sci.*, 2010, **3**, 715-726.
27. J. Zhong, F. Chen and J. Zhang, *J. Phys. Chem. C*, 2009, **114**, 933-939.
28. J. Fan, X. Jiang, H. Min, D. Li, X. Ran, L. Zou, Y. Sun, W. Li, J. Yang, W. Teng, G. Li and D. Zhao, *J. Mater. Chem. A*, 2014, **2**, 10654-10661.
29. Y. Kuwahara, K. Maki, Y. Matsumura, T. Kamegawa, K. Mori and H. Yamashita, *J. Phys. Chem. C*, 2009, **113**, 1552-1559.
30. K. Fuku, R. Hayashi, S. Takakura, T. Kamegawa, K. Mori and H. Yamashita, *Angew. Chem. Int. Ed.*, 2013, **52**, 7446-7450.
31. H.-C. Yang, H.-Y. Lin, Y.-S. Chien, J. C.-S. Wu and H.-H. Wu, *Catal. Lett.*, 2009, **131**, 381-387.
32. M. Xing, D. Qi, J. Zhang, F. Chen, B. Tian, S. Bagwas and M. Anpo, *J. Catal.*, 2012, **294**, 37-46.
33. C. Li and P. C. Stair, *Catal. Today*, 1997, **33**, 353-360.
34. Y. Wu, M. Xing and J. Zhang, *J. Hazard. Mater.*, 2011, **192**, 368-373.
35. C. Lettmann, K. Hildenbrand, H. Kisch, W. Macyk and W. F. Maier, *Appl. Catal. B: Environ.*, 2001, **32**, 215-227.
36. D.-e. Gu, Y. Lu, B.-c. Yang and Y.-d. Hu, *Chem. Commun.*, 2008, **21**, 2453-2455.
37. S. K. Parayil, H. S. Kibombo, C.-M. Wu, R. Peng, J. Baltrusaitis and R. T. Koodali, *Int. J. Hydrogen Energy*, 2012, **37**, 8257-8267.